Infectious Disease Modelling 9 (2024) 158–176

Contents lists available at ScienceDirect

Infectious Disease Modelling

journal homepage: www.keaipublishing.com/idm

Exploring the interplay between climate change and schistosomiasis transmission dynamics

Zadoki Tabo [a, b, *], Chester Kalinda [a, d], Lutz Breuer [b, c], Christian Albrecht [a]

[a] Department of Animal Ecology and Systematics, Justus Liebig University Giessen, Heinrich-Buff-Ring 26 (iFZ), 35392 Giessen, Germany
[b] Department of Landscape Ecology and Resource Management, Justus Liebig University Giessen, Heinrich-Buff-Ring 26 (iFZ), 35392 Giessen, Germany
[c] Centre for International Development and Environmental Research (ZEU), Justus Liebig University Giessen, Senckenbergstrasse 3, 35390 Giessen, Germany
[d] Bill and Joyce Cummings Institute of Global Health, University of Global Health Equity | Kigali Heights, Plot 772 KG 7 Ave. PO Box 6955, Kigali, Rwanda

ARTICLE INFO

Article history:
Received 30 July 2023
Received in revised form 7 November 2023
Accepted 16 December 2023
Available online 22 December 2023
Handling Editor: Dr Daihai He

Keywords:
Modeling
Schistosomiasis transmission
Temperature
Rainfall
Basic reproduction number
East Africa

ABSTRACT

Schistosomiasis, a neglected tropical disease caused by parasitic worms, poses a major public health challenge in economically disadvantaged regions, especially in Sub-Saharan Africa. Climate factors, such as temperature and rainfall patterns, play a crucial role in the transmission dynamics of the disease. This study presents a deterministic model that aims to evaluate the temporal and seasonal transmission dynamics of schistosomiasis by examining the influence of temperature and rainfall over time. Equilibrium states are examined to ascertain their existence and stability employing the center manifold theory, while the basic reproduction number is calculated using the next-generation technique. To validate the model's applicability, demographic and climatological data from Uganda, Kenya, and Tanzania, which are endemic East African countries situated in the tropical region, are utilized as a case study region. The findings of this study provide evidence that the transmission of schistosomiasis in human populations is significantly influenced by seasonal and monthly variations, with incidence rates varying across countries depending on the frequency of temperature and rainfall. Consequently, the region is marked by both schistosomiasis emergencies and re-emergences. Specifically, it is observed that monthly mean temperatures within the range of 22–27 °C create favorable conditions for the development of schistosomiasis and have a positive impact on the reproduction numbers. On the other hand, monthly maximum temperatures ranging from 27 to 33 °C have an adverse effect on transmission. Furthermore, through sensitivity analysis, it is projected that by the year 2050, factors such as the recruitment rate of snails, the presence of parasite egg-containing stools, and the rate of miracidia shedding per parasite egg will contribute significantly to the occurrence and control of schistosomiasis infections. This study highlights the significant influence of seasonal and monthly variations, driven by temperature and rainfall patterns, on the transmission dynamics of schistosomiasis. These findings underscore the importance of considering climate factors in the control and prevention strategies of schistosomiasis. Additionally, the projected impact of various factors on schistosomiasis infections by 2050 emphasizes the need for proactive measures to mitigate the disease's impact on vulnerable populations. Overall, this research provides

* Corresponding author. Department of Animal Ecology and Systematics, Justus Liebig University Giessen, Heinrich-Buff-Ring 26 (iFZ), 35392 Giessen, Germany.
E-mail address: tabozac@gmail.com (Z. Tabo).
Peer review under responsibility of KeAi Communications Co., Ltd.

https://doi.org/10.1016/j.idm.2023.12.003

valuable insights to anticipate future challenges and devise adaptive measures to address schistosomiasis transmission patterns.

1. Introduction

Schistosomiasis, classified as a neglected tropical disease and an infectious disease of poverty, primarily affects poor and marginalized communities with limited access to clean water and sanitation, exerting detrimental impacts on their health, economy, and social well-being (Gryseels et al., 2006). Transmission of the parasitic trematode worms *Schistosoma* spp. to humans relies on the presence of suitable freshwater intermediate hosts (IH) snails, where schistosomes undergo asexual reproduction, and humans, serving as the final hosts, where schistosomes undergo sexual reproduction (Steinmann et al., 2006). Globally, over 240 million individuals are infected with schistosomiasis, with approximately 90% of infections concentrated in sub-Saharan Africa (Bergquist et al., 2017). African regions exhibit high prevalence of *Schistosoma* species, such as *Schistosoma mansoni* transmitted by *Biomphalaria* snails, and *Schistosoma haematobium* transmitted by *Bulinus* snails (Utzinger et al., 2009).

Climate variables, including temperature and precipitation, have been shown to influence the presence of IH snails and schistosomiasis transmission (McCreesh & Booth, 2013; Stensgaard et al., 2016; Tabo et al., 2022). However, the impact of current and future climate changes on schistosomiasis development remains uncertain and subject to debate (McCreesh & Booth, 2013; Stensgaard et al., 2016; McCreesh et al., 2015; Kalinda et al., 2018). Temperature fluctuations and extreme weather events have been highlighted as crucial factors (McCreesh & Booth, 2013), and deterministic models incorporating temperature effects on IH snails' life history characteristics are recommended (Kalinda et al., 2018). Climate change also introduces variations in regional precipitation levels (Solomon, 2007), potentially altering transmission patterns and schistosomiasis onset (Codjoe & Larbi, 2016; Martens et al., 1995). In specific tropical regions, including Tanzania, Kenya, Uganda, Rwanda, Burundi, and Eastern Zambia, climate changes may create favorable environments for IH snails (McCreesh et al., 2015).

While these studies suggest a potential for ecological changes and thus changes in the transmission of schistosomiasis, they also increase the difficulties associated with characterizing the relationship between climate variability in terms of temperature and precipitation with the transmission of schistosomiasis because the relationship is likely, not linear. Therefore, modeling the impact of seasonal climate variations in temperature and precipitation is critical in determining how climate change will influence schistosomiasis infections. In this context, a few mathematical models for the transmission dynamics of schistosomes have been proposed (Chen et al., 2010; Feng et al., 2004; Kalinda et al., 2019; Li et al., 2017). For instance, Li et al. (Li et al., 2017) formulate a periodic model that shows a seasonal transmission pattern of schistosomiasis based on monthly human schistosomiasis cases in the lake and marsh areas of China while Schrader et al. (Schrader et al., 2013) incorporate host snail genetic structure and land use changes in a schistosomiasis predictive model. On the other hand, the results of Mangal et al. (Mangal et al., 2008) and Kalinda et al. (Kalinda et al., 2017a) [19] provide information on the relationship between temperature and schistosomiasis transmission for *Biomphalaria-S. mansoni* and *Bulinus-S. haematobium* systems. Although these models have been insightful in providing a framework for evaluating the impact of one climate variable on schistosomiasis transmission, it is still challenging to simultaneously understand how temperature and precipitation affect schistosomiasis transmission dynamics as a result of a changing climate (Van der Wiel & Bintanja, 2021).

The objective of this study is two-fold. Firstly, it aims to develop a new mechanistic model for schistosomiasis transmission, considering the coupled effects of temperature and rainfall. The model incorporates parameters accounting for population growth, temperature, precipitation, and the release of parasite eggs by infected individuals. Secondly, the study aims to assess the impact of temperature and rainfall variations on the frequency of schistosomiasis transmission in different geographical areas, considering seasonal variations. Regional model systems are specifically built for Tanzania, Kenya, and Uganda, countries where schistosomiasis is highly prevalent, and the climate supports the thriving of intermediate host snails, leading to widespread infections among the population.

2. Material and methods

2.1. Model formulation

The model describes the transmission dynamics of *Schistosoma* infection in a population consisting of humans, *Schistosoma* parasite eggs in the environment and free-living parasites, and snails. The population is divided into various compartments representing the different stages of the *Schistosoma* life cycle: Susceptible human compartment, $S_h(t)$, represents individuals who are susceptible to the *Schistosoma* infection. These individuals have not been infected previously and can

potentially become infected if they come into contact with the parasite. Infected human compartment $I_h(t)$, represents individuals who are currently infected with *Schistosoma*. These individuals can release parasite eggs into the environment through faces and urine and can contribute to the overall transmission dynamics. Parasite egg population compartment $E_h(t)$, represents the population of parasite eggs released into the environment by infected humans. These eggs can hatch into free-living stages of the parasite (miracidia) and infect snails. Free-living miracidia parasite compartment $M_f(t)$, are the first free-living stage of the *Schistosoma* life cycle. Miracidia can infect snails and continue their development. Snails serve as intermediate hosts for the parasite, facilitating its life cycle. Susceptible snail vector compartment $S_v(t)$, represents snails that are susceptible to becoming infected with schistosomiasis, while the infected snail vector compartment $I_v(t)$, represents snails that are currently infected with schistosomiasis. Infected snails release free-living cercaria *Schistosoma* parasite into the environment, contributing to the transmission of the infection to human. Free-living cercaria parasite compartment $C_f(t)$, this compartment represents the population of cercaria parasites, which are the final free-living stage of the *Schistosoma* life cycle. Cercariae can infect humans upon contact with contaminated water to complete the *Schistosoma* life cycle.

The model is developed based on the following assumptions and parameters, which govern the rates of transmission, infection, and mortality for each compartment, as well as the interactions between different compartments:

(A1) The human is recruited at the rate $\Lambda_1 e^{-\upsilon_1 x}$, where Λ_1 signifies the maximum birth rate or immigration rate per individual. The factor $e^{-\upsilon_1 x}$ takes into account that recruitment of individuals does not occur immediately at birth but rather at the age when they are first susceptible to infection, denoted as x. This age corresponds to a time when individuals have the opportunity to interact with contaminated water through activities such as swimming, fishing, farming, washing, and collecting water for domestic use. It is worth noting that this age may occur much earlier, for example, when babies below the age of two years are washed in infected freshwater. The parameter υ_1 represents the mortality rate among humans, and the probability of a child surviving up to the age of susceptibility is given by $1/\upsilon_1$. As for the recruitment of snails, the rate of maturation $\Lambda_2(T, R)$, is dependent on the prevailing temperature (T) and rainfall amount (R). This rate also takes into account the three stages of the snail life cycle, the number of eggs laid by each adult snail per day, and the survival rate of both the laid eggs and the juvenile (immature) snails until they reach adulthood.

(A2) Schistosomiasis is not passed down from an infected mother to her child through vertical transmission. In the model, the incidences of infection are represented by $\beta_1(T)S_hC_f$ for humans and $\beta_2(T)M_fS_v$ for snails. Here, $\beta_1(T)$ denotes the temperature-dependent rate of cercaria infection in humans, reflecting how the infection rate varies with temperature. Similarly, $\beta_2(T)$ represents the temperature-dependent rate of miracidia infection on snails, indicating the infection rate's dependence on temperature.

(A3) The natural mortality rates for various components in the schistosomiasis system are denoted as υ_1 for humans, υ_2 for snails, $d_v(T)$ for parasite eggs, $\upsilon_3(T)$ for miracidia, and υ_4 for cercaria. Disease-related mortality rates specific to humans and snails are represented as δ_1 and $\delta_2(T)$, respectively. It is important to note that the rates $d_v(T)$, $\upsilon_3(T)$, and $\delta_2(T)$ are temperature-dependent parameters, meaning they vary with changes in temperature. The model assumes that excreta (urine and/or feces), which includes parasite eggs, are either directly released into the freshwater or find their way into it. Infected humans, on average, excrete ρ stools per day, with each gram of stool containing an average number of eggs denoted as θ_h. The occurrence of miracidia is a result of the fact that, on average, N_E miracidia hatch from each egg, and the rate at which the eggs hatch is represented as ω_1. Additionally, infected snails shed cercariae at a rate of ω_2. Fig. 1 illustrates the transmission diagram of Schistosomiasis.

The mathematical model equation (1) is developed based on Fig. 1.

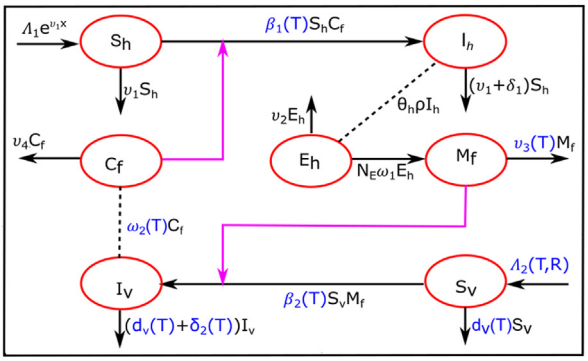

Fig. 1. Schistosomiasis transmission diagram depicting the life cycle stages of *Schistosoma*, interactions with human hosts and IH snails. Disease transmission parameters influenced by temperature and precipitation are highlighted in blue.

$$\left.\begin{aligned}
\frac{dS_h}{dt} &= \Lambda_1 e^{-\upsilon_1 x} - \beta_1(T) S_h C_f - \upsilon_1 S_h \\
\frac{dI_h}{dt} &= \beta_1(T) S_h C_f - (\upsilon_1 + \delta_1) I_h \\
\frac{dE_h}{dt} &= \theta_h \rho I_h - (\omega_1 + \upsilon_2) E_h \\
\frac{dM_f}{dt} &= N_E \omega_1 E_h - \upsilon_3(T) M_f \\
\frac{dS_v}{dt} &= \Lambda_2(T,R) - \beta_2(T) M_f S_v - d_v S_v \\
\frac{dI_v}{dt} &= \beta_2(T) M_f S_v - (d_v(T) + \delta_2(T)) I_v \\
\frac{dC_f}{dt} &= \omega_2(T) I_v - \upsilon_4 C_f
\end{aligned}\right\} \quad (1)$$

In this study, we adopt an autonomous dynamic model equation (1) to investigate the general dynamic effects of climate-driven systems on schistosomiasis. The spatial characteristics of our autonomous model output are determined by parameterization using temperature and rainfall values dependent on temperature and/or rainfall-related parameters.

2.2. Steady states and reproduction number of the model

We show that model (1) has both disease-free and endemic equilibria. The disease-free equilibrium represents a state in which the population remains free from the infection, indicating the absence of active transmission. In contrast, the endemic equilibrium represents a persistent state of disease transmission within the population, indicating an ongoing and stable level of infection. The disease-free equilibrium is crucial as it serves as a benchmark to evaluate the effectiveness of control measures. On the other hand, the endemic equilibrium provides insights into the persistence and stability of schistosomiasis transmission. In our model, the basic reproduction number (R_0) plays a fundamental role. It quantifies the average number of new infections caused by a single infectious individual in a susceptible population (Diekmann et al., 1990). If R_0 is greater than 1, it indicates that schistosomiasis has the potential to emerge, spread, and persist within the population. In contrast, if R_0 is less than 1, it suggests that, on average, less than one new case of schistosomiasis is generated during the infectious period, making the disease-free equilibrium more likely. The interplay between these equilibrium conditions and their impact under climate factors such as temperature and rainfall is crucial to forming public health strategies, as it gives insight into disease potential, the effectiveness of control measures, and the likelihood of achieving disease elimination.

We are able to calculate R_0 using model equation (1) of the autonomous dynamic model, as long as we disregard the temporal variations in temperature and rainfall (see e.g. Okuneye & Gumel, 2017; Parham & Michael, 2010). Thus, following the approach by Driessche and Watmough, (Driessche & Watmough, 2002) and Diekmann et al. (Diekmann et al., 1990), the next-generation technique is employed to determine the dominant eigenvalue, which represents the value of R_0 in the model (1). It can be expressed as:

$$R_0 = \sqrt{\left(\frac{\beta_1(T) N_E \omega_1 \theta_h \rho \Lambda_1 e^{-\upsilon_1 x}}{\upsilon_1 \upsilon_4 (d_v(T) + \delta_2(T))(\omega_1 + \upsilon_2)}\right) \cdot \left(\frac{\beta_2(T) \omega_2(T) \Lambda_2(T,R)}{\upsilon_3(T) d_v(T)\ (\upsilon_1 + \delta_1)}\right)} \quad (2)$$

Furthermore, R_0 can be represented as $R_0(T,R) = \sqrt{R_0^{S_h} R_0^{S_v}}$ where $R_0^{S_h}(T) = \frac{\beta_1(T) N_E \omega_1 \theta_h \rho(T) \Lambda_1 e^{-\upsilon_1 x}}{\upsilon_1 \upsilon_4 (d_v(T) + \delta_2(T))(\omega_1 + \upsilon_2)}$ and $R_0^{S_v}(T,R) = \frac{\beta_2(T) \omega_2(T) \Lambda_2(T,R)}{\upsilon_3(T) d_v(T)\ (\upsilon_1 + \delta_1)}$ under the square root, representing new cases of schistosomiasis infections in humans per infectious snail and cases of schistosomiasis infections in snails per infectious human, respectively. Thus, we obtained the standard expression of $R_0(T,R)$ under static environmental conditions where temperature and rainfall are constant at a given time. To determine the disease-free equilibrium E_0, we can set the equations of the model (1) to zero and solve for the respective variables when no infective compartments exist, i.e. $I_h = E_h = M_f = I_v = C_f = 0$, defined as:

$E_0 = (S_h', I_h', E_h', M_f', S_v', I_v', C_c') = \left(\frac{\Lambda_1 e^{-\upsilon_1 x}}{\upsilon_1}, 0, 0, 0, \frac{\Lambda_2(T,R)}{d_v}, 0, 0\right)$, E_0 always exists in a certain region $\Omega \in \mathscr{R}^7_{+0}$.

2.2.1. Local stability of the disease-free steady state, E_0

In this study, we analyze the local stability conditions of the disease-free equilibrium, E_0, in the model (1) based on the following theorem:

Theorem 3.1. *The disease-free steady state, E_0, in model (1) is locally asymptotically stable when $R_0 < 1$, and it is unstable when $R_0 > 1$.*

We present a proof for this theorem by demonstrating that all eigenvalues of the Jacobian matrix J(A) in (3), evaluated at E_0, are negative.

$$J(A) = \begin{pmatrix} -\upsilon_1 & 0 & 0 & 0 & 0 & 0 & -\beta_1 S_h' \\ 0 & -(\upsilon_1 + \delta_1) & 0 & 0 & 0 & 0 & \beta_1 S_h' \\ 0 & \rho\theta_h & -(\omega_1 + \upsilon_3) & 0 & 0 & 0 & 0 \\ 0 & 0 & N_E\omega_1 & -\upsilon_3 & 0 & 0 & 0 \\ 0 & 0 & 0 & -\beta_2 S_v' & -d_v & 0 & 0 \\ 0 & 0 & 0 & \beta_2 S_v' & 0 & -(d_v + \delta_2) & 0 \\ 0 & 0 & 0 & 0 & 0 & \omega_2 & -\upsilon_4 \end{pmatrix} \tag{3}$$

The Jacobian matrix $J(A)$ has seven eigenvalues, two of which by inspection in the first and fifth columns are $-\upsilon_1$ and $-d_v$. We exclude columns one and five with the corresponding rows and the resultant matrix gives the characteristic equation (4) whose roots are the remaining five eigenvalues of the Jacobian matrix

$$a_0\lambda^5 + a_1\lambda^4 + a_2\lambda^3 + a_3\lambda^2 + a_4\lambda + a_5 = 0 \tag{4}$$

where,

$$a_0 = 1, a_1 = (\upsilon_1 + \delta_1) + (\omega_1 + \upsilon_3) + \upsilon_3 + (d_v + \delta_2) + \upsilon_4$$

$$a_2 = \upsilon_3\upsilon_4 + (d_v + \delta_2)(\upsilon_3 + \upsilon_4) + ((\upsilon_1 + \delta_1) + (\omega_1 + \upsilon_3))((d_v + \delta_2) + (\upsilon_3 + \upsilon_4)) + (d_v + \delta_2)(\upsilon_3 + \upsilon_4),$$

$$a_3 = \upsilon_3\upsilon_4(d_v + \delta_2) + (\upsilon_3\upsilon_4 + (d_v + \delta_2)(\upsilon_3 + \upsilon_4))((\upsilon_1 + \delta_1) + (\omega_1 + \upsilon_3)) + (\upsilon_1 + \delta_1)(\omega_1 + \upsilon_3)((d_v + \delta_2) + (\upsilon_3 + \upsilon_4)),$$

$$a_4 = \upsilon_3\upsilon_4(d_v + \delta_2)((\upsilon_1 + \delta_1) + (\omega_1 + \upsilon_3)) + (\upsilon_1 + \delta_1)(\omega_1 + \upsilon_3)(\upsilon_3\upsilon_4 + (d_v + \delta_2)(\upsilon_3 + \upsilon_4)),$$

$$a_4 = \upsilon_3\upsilon_4(\upsilon_1 + \delta_1)(\omega_1 + \upsilon_3)(d_v + \delta_2).$$

The local stability of equilibrium point E_0 is determined by satisfying the conditions that $a_i > 0$ ($i = 1, 2, 3, 4, 5$), and $a_1a_2a_3a_4 + a_3a_5 + a_4a_5 > a_1a_2a_5 + a_1a_4^2 + a_3^2a_5$, based on the Routh-Hurwitz stability criteria for characteristic equation (4).

2.2.2. Global stability of the disease-free steady state, E_0

In accordance with Castillo-Chavez et al. (Castillo-Chavez, Feng, & Huang, 2002), our investigation focuses on the global stability of the disease-free steady state by reformulating model (1) into the following form:

$$\begin{cases} \dfrac{dX}{dt} = F(X, Z) \\ \dfrac{dZ}{dt} = G(X, Z), G(X, 0) = 0 \end{cases}$$

Here, $X = (S_h, S_v)$ represents the susceptible population, while $Z = (I_h, I_v, E_h, M_f, C_f)$ represents the infected population that is not infectious (I_h, I_v, E_h) and the infectious population (M_f, C_f). We set , $U_0 = (\tilde{X}, 0) = (\Lambda_1 e^{-\upsilon_1 x}/\upsilon_1, 0, 0, 0, \Lambda_2(T, R)/d_v, 0, 0)$ as the disease-free equilibrium of the model (1) and Theorem 3.2 holds.

Theorem 3.2. *The fixed point $U_0 = (\tilde{X}, 0)$ is globally asymptotically stable if $R_0 \leq 1$, and if the two conditions (B1) and (B2) below are fulfilled*:

(B1) $\frac{dX}{dt} = F(X, 0)$, $\tilde{X}$ is globally asymptotically stable

(B2) $G(X, Z) = AZ - \widehat{G}(X, Z)$ and $\widehat{G}(X, Z) \geq 0$ for (X, Z) ∈ R_+^7.*where $A = D_zG(\tilde{X}, 0)$ is an M-matrix and R_+^7 is the region in which model (1) makes biological sense.*

Proof: In our model (1), we have

$$F(X,0)=\begin{pmatrix}\Lambda_1 e^{-\upsilon_1 x}-\upsilon_1 S_h\\ \Lambda_2(T,R)-d_v S_v\end{pmatrix}$$

$$A=\begin{pmatrix}-(\upsilon_1+\delta_1) & 0 & 0 & 0 & \beta_1 S_h'\\ 0 & -(d_v+\delta_2) & 0 & \beta_2 S_v' & 0\\ \theta_h\rho & 0 & -(\omega_1+\upsilon_3) & 0 & 0\\ 0 & 0 & N_E\omega_1 & -\upsilon_4 & 0\\ 0 & \omega_2 & 0 & 0 & -\upsilon_5\end{pmatrix}$$

$$\widehat{G}(X,Z)=G(X,Z)-AZ=[0\quad 0\quad 0\quad 0\quad 0]^T=0.$$

In the computation, we show that

$$S_h(t)=\frac{\Lambda_1 e^{-\upsilon_1 x}}{\upsilon_1}+\left(S_h(0)-\frac{\Lambda_1 e^{-\upsilon_1 x}}{\upsilon_1}\right)e^{-\upsilon_1 t}\text{ and }S_v(t)=\frac{\Lambda_2(T,R)}{d_v}+\left(S_v(0)-\frac{\Lambda_2(T,R)}{d_v}\right)e^{-d_v t}$$

where $S_h(t)$ and $S_v(t)$, approach $\frac{\Lambda_1 e^{-\upsilon_1 x}}{\upsilon_1}$ and $\frac{\Lambda_2(T,R)}{d_v}$ as $t\to\infty$, respectively. The convergence of the solutions is global in R_+^7. Thus, $\tilde{X}$ is globally asymptotically stable, satisfying condition (A1). Moreover, matrix A is an M-matrix satisfying (A2) and as a result, Theorem 3.3 holds.

2.2.3. Existence and stability of the endemic steady state, $\boldsymbol{E_1}$

The endemic equilibrium point E_1 can be found by setting the equations of model (1) to zero, considering all compartments. The endemic equilibrium point exists when $R_0>1$ and the stability conditions for the disease-free equilibrium are not satisfied. Thus, $E_1=(S_h^*,I_h^*,E_h^*,M_f^*,S_v^*,I_v^*,C_f^*)$ and we express it in terms of I_v^* where

$$S_h^*(I_v^*)=\frac{\upsilon_4\Lambda_1 e^{-\upsilon_1 x}}{\beta_1\omega_2 I_v^*+\upsilon_1\upsilon_4}$$

$$I_h^*(I_v^*)=\frac{\beta_1\omega_2\Lambda_1 e^{-\upsilon_1 x}I_v^*}{(\beta_1\omega_2 I_v^*+\upsilon_1\upsilon_4)(\upsilon_1+\delta_1)}$$

$$E_h^*(I_v^*)=\frac{\beta_1\omega_2\rho\theta_h\Lambda_1 e^{-\upsilon_1 x}I_v^*}{(\omega_1+\upsilon_2)(\beta_1\omega_2 I_v^*+\upsilon_1\upsilon_4)(\upsilon_1+\delta_1)}$$

$$M_f^*(I_v^*)=\frac{\beta_{1\omega_1}\omega_2\rho\theta_h N_E\Lambda_1 e^{-\upsilon_1 x}I_v^*}{\upsilon_3(\omega_1+\upsilon_2)(\beta_1\omega_2 I_v^*+\upsilon_1\upsilon_4)(\upsilon_1+\delta_1)}$$

$$S_v^*(I_v^*)\frac{(\beta_1\omega_2 I_v^*+\upsilon_1\upsilon_4)\Lambda_2}{\upsilon_1\upsilon_4(d_v+\delta_2)R_0^2 I_v^*+d_v(\beta_1\omega_2 I_v^*+\upsilon_1\upsilon_4)}$$

$$C_f^*(I_v^*)=\frac{\omega_2}{\upsilon_4}I_v^*$$

By setting dI_v/dt to zero in equations of model (1) and substituting S_v^* and I_h^*, we obtain the following expression:

$$\left(\mathrm{p}_1 I_v^{*2}+\mathrm{p}_2 I_v^*+\mathrm{p}_3\right)I_v^*=0 \tag{5}$$

where $\mathrm{p}_1=\beta_1\omega_2(d_v+\delta_2)$, $\mathrm{p}_2=\mathrm{p}_1\upsilon_2(\upsilon_4(d_v+\delta_2-R_0^2)-2\upsilon_2)$ and $\mathrm{p}_3=\upsilon_1\upsilon_2(d_v+\delta_2)[\upsilon_1\upsilon_4(d_v+\delta_2)(1-\upsilon_1\upsilon_2R_0^2)+\upsilon_1\upsilon_2]$. Equation (5) has a solution where $I_v^*=0$, corresponding to the disease-free equilibrium. Additionally, the existence of an endemic equilibrium point is ensured if $R_0>1$ and $I_v^*\in\mathscr{R}_{+0}$, where I_v^* is given by $I_v^*=\frac{\mathrm{p}_2\pm\sqrt{\mathrm{p}_2{}^2-4\mathrm{p}_1\mathrm{p}_3}}{2\mathrm{p}_1}$.

2.2.4. The local stability of the endemic steady state

The condition which determines the threshold for the local stability of the endemic equilibrium, taking into account the respective parameters and values in the model is provided by the following theorem 3.3.

Theorem 3.3. *The endemic equilibrium E_1 is locally asymptotically stable if the basic reproduction number $R_0 > 1$, and the bifurcation parameter $\omega_1 = \omega_1^*$ satisfies $\omega_1 = \omega_1^* > \frac{\upsilon_1\upsilon_2\upsilon_3\upsilon_4 d_v(d_v+\delta_2)(\upsilon_1+\delta_1)}{\beta_1\beta_2\omega_2 N_E\theta_h\rho\Lambda_2\Lambda_1 e^{-\upsilon_1 x}-\upsilon_1\upsilon_3\upsilon_4 d_v(d_v+\delta_2)(\upsilon_1+\delta_1)}$.*

Proof.

We employ the manifold theorem described in Castillo-Chavez and Song, (Castillo-Chavez & Song, 2004), first, we define the variables as follows: $S_h = x_1, I_h = x_2, E_h = x_3, M_f = x_4, S_v = x_5, I_v = x_6, C_f = x_7$ and the model (1) is then transformed into the form $\frac{dx_i}{dt} = \dot{x}_i = (\dot{x_1}, \dot{x_2}\dot{x_3}, \dot{x_4}, \dot{x_5}, \dot{x_6}, \dot{x_7})^T$, where

$$\left.\begin{aligned} \dot{x_1} &:= f_1 = \Lambda_1 e^{-\upsilon_1\tau} - \beta_1 x_1 x_7 - \upsilon_1 x_1\ ;\ \dot{x_2} := f_2 = \beta_1 x_1 x_7 - (\upsilon_1+\delta_1)x_2;\\ \dot{x_3} &:= f_3 = \rho\theta_h x_2 - (\omega_1^* + \upsilon_2)x_3;\ \dot{x_4} := f_4 = N_E\omega_1^* x_3 - \upsilon_3 x_4;\\ \dot{x_5} &:= f_5 = \Lambda_2(T,R) - \beta_2 x_4 x_5 - d_v x_5;\ \dot{x_6} := f_6 = \beta_2 x_4 x_5 - (d_v+\delta_2)x_6;\\ \dot{x_7} &:= f_7 = \omega_2 x_6 - \upsilon_4 x_7 \end{aligned}\right\} \tag{6}$$

The transformed model (6) has the same disease-free equilibrium and the reproduction number R_0 as for model (1) above. Let the critical miracidia shedding be $\omega_1 = \omega_1^* = \frac{\upsilon_1\upsilon_2\upsilon_3\upsilon_4 d_v(d_v+\delta_2)(\upsilon_1+\delta_1)}{\beta_1\beta_2\omega_2 N_E\theta_h\rho\Lambda_2\Lambda_1 e^{-\upsilon_1 x}-\upsilon_1\upsilon_3\upsilon_4 d_v(d_v+\delta_2)(\upsilon_1+\delta_1)}$ as the bifurcation parameter at $R_0 = 1$. The linearized model (6) evaluated at disease-free equilibrium $(x_1^* = \Lambda_1 e^{-\upsilon_1 x}/\upsilon_1, x_2^* = 0, x_3^* = 0, x_4^* = 0, x_5^* = \Lambda_2(T,R)/d_v, x_6^* = 0, x_7^* = 0)$ with $\omega_1 = \omega_1^*$, has a simple eigenvalue associated with a right eigenvector $\boldsymbol{u} = (u_1, u_2, u_3, u_4)^T$ and a left eigenvector $\boldsymbol{v} = (\upsilon_1, \upsilon_2, \upsilon_3, \upsilon_4)$ satisfying $\boldsymbol{u}.\boldsymbol{v} = \mathbf{1}$, where

$$u_1 = \frac{-\beta_1 x_1^*}{\upsilon_1}u_7\ , u_2 = \frac{\beta_1 x_1^*}{(\upsilon_1+\delta_1)}u_7\ , u_3 = \frac{\beta_1\rho\theta_h x_1^*}{(\upsilon_1+\delta_1)(\omega_1^*+\upsilon_2)}u_7\ , u_4 = \frac{\beta_1\omega_1^*\rho\theta_h N_E x_1^*}{(\upsilon_1+\delta_1)(\omega_1^*+\upsilon_2)}u_7\ ,$$

$$u_5 = \frac{\beta_1\beta_2\omega_1^*\rho\theta_h N_E x_1^* x_5^*}{\upsilon_3 d_v(\upsilon_1+\delta_1)(\omega_1^*+\upsilon_2)}u_7\ , u_6 = \frac{\beta_1\beta_2\omega_1^*\rho\theta_h N_E x_1^* x_5^*}{\upsilon_3(d_v+\delta_2)(\upsilon_1+\delta_1)(\omega_1^*+\upsilon_2)}u_7\ , u_7 > 0$$

$$\upsilon_1 = -\upsilon_1, \upsilon_2 = \frac{\rho\theta_h}{(\upsilon_1+\delta_1)}\upsilon_3\ , \upsilon_3 > 0, \upsilon_4 = \frac{(\omega_1^*+\upsilon_2)}{N_E\omega_1^*}\upsilon_3\ , \upsilon_5 = 0, \upsilon_6 = \frac{\upsilon_3(\omega_1^*+\upsilon_2)}{N_E\omega_1^*\beta_2 x_5^*}\upsilon_3\ ,$$

$$\upsilon_7 = \frac{\upsilon_3(\omega_1^*+\upsilon_2)(d_v+\delta_2)}{\omega_1\omega_2\beta_2 N_E x_5^*}\upsilon_3\ .$$

We compute the values of coefficients a and b according to Castillo-Chavez and Song, (Castillo-Chavez & Song, 2004), and it is shown that at the disease-free equilibrium, the second-order non-zero partial derivatives associated with model (4) are as follows:

$$\frac{\partial^2 f_1}{\partial x_1\partial x_7} = -\beta_1, \frac{\partial^2 f_2}{\partial x_1\partial x_7} = \beta_1, \frac{\partial^2 f_5}{\partial x_4\partial x_5} = -\beta_2, \frac{\partial^2 f_6}{\partial x_4\partial x_5} = \beta_2, \frac{\partial^2 f_3}{\partial x_3\partial\omega_1^*} = -1, \frac{\partial^2 f_4}{\partial x_3\partial\omega_1^*} = N_E$$

The computation results in

$$a = \frac{\upsilon_3\delta_1\beta_1^2(d_v+\delta_2)(\omega_1^*+\upsilon_2)x_1^*}{\omega_1\omega_2\beta_2 N_E(\upsilon_1+\delta_1)x_1^*}u_7 > 0 \tag{7}$$

$$b = \frac{\beta_1\rho\theta_h\left(N_E^2\omega_1^* - 1\right)x_1^*}{(\upsilon_1+\delta_1)(\omega_1^*+\upsilon_2)}u_7\ \upsilon_3 \tag{8}$$

These results in equations (7) and (8) indicate the existence of an endemic equilibrium point that is locally asymptotically stable ($a > 0, b > 0$) when $N_E^2\omega_1^* > 1$. Conversely, the equilibrium is unstable when $N_E^2\omega_1^* < 1$. The proof of Theorem 3.3 is thus completed

2.3. Model datasets and model applicability

To evaluate the suitability and applicability of the model, demographic and climatological data were collected from three East African countries: Uganda, Kenya, and Tanzania (Home, 2023). These countries, located in the tropical region, are recognized for their endemicity of schistosomiasis and display a wide range of climatic conditions and parameters that have a substantial impact on disease transmission. The population data for the three countries were obtained from the most recent UN demographic estimates (https://worldpopulationreview.com/countries) and World Bank statistics (https://data.worldbank.org/indicator/sp.dyn.le00.in?). These data sources provided valuable information for estimating certain non-temperature and non-rainfall parameters in the model. For example, Uganda has a population of about 47,264,873 people with a life expectancy of 58.5 years. Consequently, in a disease-free steady state, the susceptible population is represented by $S_h' = \frac{\Lambda_1 e^{-\upsilon_1 x}}{\upsilon_1} = 47,264,873$, where $\upsilon_1 = 1/((58.5 \times 365)) = 0.0000468$ per day, resulting in a daily recruitment rate of $\Lambda_1 = 2212$ individuals. Similarly, Kenya has a population of 54,039,625 with a life expectancy of 64 years, yielding $\upsilon_1 = 1/((64 \times 365)) = 0.0000428$ and $\Lambda_1 = 2,313$ new infections per day. Tanzania, with a population of 65,519,777 and a life expectancy of 62.6 years, has $\upsilon_1 = 1/((62.6 \times 365)) = 0.0000444$ and $\Lambda_1 = 2,909$ new infections per day. The other non-temperature and non-rainfall parameters x, δ_1, and υ_2 of the model are derived from the literature. For instance, we assume that schistosomiasis typically first infects a child at the age of two (2), corresponding to $x = 2 \times 365 = 730$ days. The lifespan of an adult *Schistosoma* worm in a human host varies from 3 to 10.5 years according to Fulford et al. (Fulford et al., 1995) and Colley et al. (Colley et al., 2014), resulting in a range of δ_1 values from $1/(10.5 \times 365) \approx 0.000268$ to $1/(3 \times 365) \approx 0.000913$ per day. Additionally, the *Schistosoma* parasite egg remains viable for up to 7 days, hence $\upsilon_2 = 1/7 = 0.14286$ represents the per capita death rate of the parasite eggs (Gryseels et al., 2006; Michaels & Prata, 1968).

Furthermore, we determined temperature-dependent parameters using data from field and laboratory studies by Mangal et al. (Mangal et al., 2008) (SI Table S1) and Kalinda et al. (Kalinda et al., 2017a) (SI Table S2). These studies have demonstrated that the activity of both snails and *Schistosoma* parasites is optimized within the temperature range of 20–35 °C. We fitted temperature regression curves up to five degrees to these data and selected the results with the highest adjusted R-squared value, R-Sq (adj), along with the corresponding equations. Additionally, we developed functions for temperature- and precipitation-dependent parameters that influence snail recruitment, following methodologies described in (Okuneye & Gumel, 2017; Parham & Michael, 2010). These equations were applied to fit the climate data of the three countries. For parameters not commonly reported, we made informed assumptions based on expertise and general knowledge of vector and disease dynamics. The remaining parameters were obtained from the literature (Table 1).

Seasonal climate data for each country were obtained from the most recent World Bank Climatology (Home, 2023, Table 2). The current temperature range and rainfall variation were 21–33 °C and 5–166 mm, respectively, based on the current climate data presented in Table 2. However, it is projected that by 2050, East Africa will experience a temperature increase of approximately 2 °C (Home, 2023) due to global warming, and monthly rainfall will vary between 180 and 188 mm (Home, 2023; Ngoma et al., 2021; Najjuma et al., 2021). Based on these projections, we extrapolated rainfall ranges from 4 to 200 mm and a temperature range of 27–35 °C to represent adverse conditions for schistosomiasis transmission in future scenarios. We divided these ranges into intervals to account for future climate variability in different regions. By using the partial rank correlation coefficient (PRCC) test, we identified critical parameters that are most sensitive to disease transmission. This allowed us to analyze the relationship between climate change variables such as temperature and precipitation and the transmission of schistosomiasis, enabling us to simulate infections under hypothetical future conditions.

The numerical analyses and simulations to determine and estimate parameters and expressions for temperature and precipitation-dependent are carried out in the R statistical environment version 4.0.3 (Team, 2018), using the primary R package ODE solver Version 1.10–4 for solving ordinary differential equations (Soetaert et al., 2010). The model parameters in

Table 1
Temperature in-variant parameters, their definitions, values per day, and sources. If a parameter is computed using the references listed in the parameter estimation section, it is referenced as “Estimated”; otherwise, it is “Assumed” based on knowledge and expertise).

Symbol	Definition	Baseline value	Values/day	References
Λ_1	Human reproduction rate	2561	2213–2909	Estimated
τ	Age at first infection in a child	730	730	Estimated
δ_1	Human mortality due to infection	0.000591	0.000268-0.000913	Estimated
υ_1	Human mortality rate	0.0000448	0.0000428–0.0000468	Estimated
ρ	Portion of stool per person	115	70–160 g	Liang et al. (2005)
θ_h	Number of eggs per gram of stool	262	10-513 g^{-1}	Liang et al. (2005)
ω_1	Miracidia shedding rate	0.00232	0.00232	Estimated
υ_2	Parasite egg mortality rate	0.14286	0.14286	Estimated
υ_4	Cercaria mortality rate	1	1	Mangal et al. (2008)
N_E	Number of miracidia per parasite egg	500	500	Mangal et al. (2008)
P_E	Maximum survival probability of egg	0.8	0.8	Assumed
P_j	Maximum survival probability of juvenile	0.9	0.9	Assumed
R_m	Rainfall threshold	250	250 mm	Assumed

Table 2
The monthly mean, maximum (max.) temperatures (°C) and rainfall (mm) for Uganda (UG), Kenya (KY) and Tanzania (TZ) from World Bank Climatology Report (Home, 2023).

Countries		Jan	Feb	Mar	Apr	May	Jun	Jul	Aug	Sept	Oct	Nov	Dec
UG	Mean	23.93	24.49	24.45	23.81	23.21	22.71	22.34	22.66	22.91	23.14	23.32	23.16
	Max.	31.09	31.61	30.99	29.62	28.79	28.46	28.09	28.47	28.98	29.32	29.64	29.81
	Rainfall	50.67	48.82	108.5	157.97	148.23	91.83	91.47	119.33	121.33	154.59	116.02	73.55
KY	mean	25.5	26.28	26.74	26.11	25.05	24.06	23.44	23.83	24.59	25.37	25.08	25.03
	Max.	32.23	33.22	33.25	31.71	30.43	29.59	28.94	29.4	30.75	31.36	30.73	31.18
	Rainfall	31.78	25.36	63.53	134.19	92.52	35.61	31.81	35.06	28.09	77.44	110.48	60.20
TZ	mean	23.59	23.7	23.68	23.02	22.28	21.09	20.58	21.64	22.94	24.02	24.07	23.69
	Max.	28.68	29.02	28.92	28.01	27.61	27.08	26.89	28.01	29.38	30.24	29.75	28.8
	Rainfall	154.76	140.2	165.76	140.61	56.29	10.97	4.99	7.29	15.18	32.55	84.85	144.4

Table 1, the equations for climatic changes in temperature and precipitation from the fitted curves, and climatology data in Table 2 are used and the results are presented in Section 4 below.

3. Results and numerical simulations

3.1. Impact of temperature and/or rainfall on specific parameters and R_0

The fitted curves derived from Table S1 (Mangal et al., 2008) and Table S2 (Kalinda et al., 2017a) establish the relationship between temperature and/or rainfall with each specific parameter, while the expression in equation (2) represents the relationship between R_0 and the individual parameter. By combining these relationships, we can evaluate the impact of temperature changes on the value of R_0 for specific parameters. First, it is evident from R_0 expression in equation (2) that increasing values of $\beta_1(\mathrm{T})$, $\omega_2(\mathrm{T})$, $\beta_2(\mathrm{T})$, and $\Lambda_2(T,R)$ leads to an increase in R_0, while increasing values of $d_v(T)$, $\delta_2(\mathrm{T})$, and $\upsilon_3(\mathrm{T})$ result in a decrease in R_0. Second, we can directly observe the impact of temperature on the transmission dynamics represented by R_0. For instance, the fitted curve for the human infection rate $\beta_1(\mathrm{T})$ is given as

$$\beta_1(\mathrm{T}) = 6.300 \times 10^{-3} T - 0.0980, \tag{9}$$

where, $d\beta_1(T)/dT > 0$, indicating that human cercaria infection increases linearly with temperature. Consequently, $\frac{dR_0}{dT} = \frac{dR_0}{d\beta_1}.\frac{d\beta_1}{dT} > 0$, implying that the transmission rate of schistosomiasis will increase with increasing temperature. Moreover, the fitted curve for shedding of cercariae $\omega_2(T)$ is give as

$$\omega_2(\mathrm{T}) = 394.9\, T - 5584.1, \tag{10}$$

and $d\omega_2(\mathrm{T})/dT > 0$. As a result, cercaria is shed more often in places with increasing temperature ranges of 20–35 °C. Consequently, $\frac{dR_0}{dT} = \frac{dR_0}{d\omega_2}.\frac{d\omega_2}{dT} > 0$, which shows that R_0 increases with increasing temperature. The fitted curve for the snail infection rate, $\beta_2(\mathrm{T})$, is given by:

$$\beta_2(\mathrm{T}) = -9.830 \times 10^{-6} T^2 + 6.148 \times 10^{-4} T - 0.008257, \tag{11}$$

This curve describes a nonlinear relationship between $\beta_2(\mathrm{T})$ and temperature. The maximum snail infection rate, according to this curve, is $\beta_2(T) = 0.00136$, which occurs at a temperature of $T = 31.3^{o}C$. Consequently, snail infections increase and decrease in locations with climatic fluctuations between 20.0 to 31.3 °C and 31.3–35.0 °C, respectively. Therefore, $\frac{dR_0}{dT} = \frac{dR_0}{d\beta_2}.\frac{d\beta_2}{dT}$ shows that the transmission is increasing between 20.0 and 31.3 °C and decreasing between 31.3 and 35.0 °C. Furthermore, the fitted curve for the snail mortality rate, $d_v(T)$, is defined as follows:

$$d_v(T) = 1.120 \times 10^{-4} T^2 - 5.208 \times 10^{-3} T + 0.06332 \tag{12}$$

The result of $dd_v(T)/dT$ shows a minimum at 23.3 °C, indicating that for temperatures between 23.3 and 35 °C, $d_v(T)$ increases. On the other hand, for temperatures between 20 and 23.3 °C, $d_v(T)$ decreases. Therefore, it follows from the formula $\frac{dR_0}{dT} = \frac{dR_0}{dd_v}.\frac{dd_v}{dT}$ that the transmission decreases for temperatures between 23.3 and 35.0 °C and increases between 20.0 and 23.3 °C.

In addition, the fitted curve for snail infection mortality rate is expressed as:

$$\delta_2(\mathrm{T}) = 8 \times 10^{-5} T^2 - 1.22 \times 10^{-3} T - 0.00545 \tag{13}$$

From equation (13), it can be observed that $d\delta_2(T)/dT > 0$. Therefore, δ_2(T) increases with increasing temperature. Consequently, the transmission indicator R_0 also increases with temperature in the range of 20 to 35 °C, as indicated by $\frac{dR_0}{dT} = \frac{dR_0}{d\delta_2}.\frac{d\delta_2}{dT} > 0$. On the other hand, the fitted curve for miracidia mortality rate, υ_3(T), is mathematically represented as:

$$\upsilon_3(\mathrm{T}) = 0.18340\mathrm{T} - 1.71, \tag{14}$$

Similarly, it can be observed that $d\upsilon_3(T)/dT > 0$. Consequently, in areas where temperatures fluctuate between 20 and 35 °C, the infection of snails with miracidia increase and according to the expression $\frac{dR_0}{dT} = \frac{dR_0}{d\upsilon_3}.\frac{d\upsilon_3}{dT}$, the prevalence of the disease (R_0) also rises within the same temperature range.

Moreover, the revised formulation for the snail recruitment rate, $\Lambda_2(T,R)$, assumes that snails can withstand variations in temperature and precipitation throughout their life stages, starting from the egg stage to the juvenile and adult stages. It is mathematically represented as:

$$\Lambda_2(T,R) = \frac{E_v(T)}{d_v(T)}.P_E(R).P_J(T,R).\frac{1}{t_S(T)}, \tag{15}$$

In equation (15), $E_v(T)$ represents the number of snail eggs per snail per day, $1/d_v(T)$ denotes the average lifespan of adult snails, $P_E(T)$ and $P_J(T,R)$ represent the daily survival probabilities of eggs and juvenile snails respectively, and $t_S(T)$ represents the total time required for a snail to develop from an egg to an adult. It is evident from equation (15) that $\Lambda_2(T,R)$, increases with higher values of $E_v(T)$, $P_E(R)$, and $P_J(T,R)$, while increasing values of $d_v(T)$, and $t_S(T)$ result in a decrease in $\Lambda_2(T,R)$. The impact of temperature and/or rainfall on a specific parameter and snail recruitment rate in equation (15) can be summarized as follows:

The relationship between the number of snail eggs $E_v(T)$, and temperature T, as determined from the equation that best fits the data in Table S2, can be expressed as

$$E_v(T) = -0.09601T^2 + 5.10696T - 52.52573 \tag{16}$$

By analyzing $dE_v(T)/dT$, it can be observed that $E_v(T)$ increases until it reaches a peak at approximately 27 °C, after which it starts to decrease. Consequently, based on the formula $\frac{d\Lambda_2(T,R)}{d_T} = \frac{d\Lambda_2(T,R)}{dE_v(T)}.\frac{dE_v(T)}{dT}$, the snail recruitment rate $\Lambda_2(T,R)$ increases within the temperature range of 20 to 27 °C and decreases within the range of 27 to 35 °C.

Additionally, it is important to note that the survival rates of eggs and juvenile snails are influenced independently by both rainfall and temperature (Parham & Michael, 2010). Therefore, we can express $P_J(T,R)$ as the product of temperature-dependent daily juvenile snail survival probability, $P_J(T)$, and rainfall-dependent survival probability, $P_J(R)$. Specifically, $P_J(T)$ is defined as $P_J(T) = e^{-\upsilon_J(T)}$, where $\upsilon_J(T)$ represents the temperature-dependent natural mortality rate of juvenile snails, obtained from a line that best fits the data (SI Table S2). Thus, $P_J(T)$ can be represented as an exponential function:

$$P_J(T) = e^{-\left(8.750\times10^{-5}T^2 - 3.762\times10^{-3}T + 0.04178\right)} \tag{17}$$

In equation (17), it can be observed that $dP_J(T)/dT$ indicates that $P_J(T)$ initially decreases to a minimum around T = 22 °C and then increases with higher temperatures. Consequently, changes in $\Lambda_2(T,R)$ will follow the same trend. In contrast, $P_i(R)$ describes the probability of survival for eggs or juvenile snails on a daily basis and in comparison to Parham and Michael, (Parham & Michael, 2010), we can express $P_i(R)$ as

$$P_i(R) = \left(4P_{Mi} \Big/ R_L^2\right)R(R_L - R), i = \{E,J\}, \tag{18}$$

Here, P_{Mi} represents the maximum daily survival probability of the egg and juvenile stages, R_L represents the maximum rainfall in the region of interest, and $R_L > R(t) > 0$. When we set $P_{Mi} = 0.8$ and $R_L = 200$ mm, it can be observed that $dP_i(R)/\,dR$ indicates that $P_i(R)$ is maximum when the total amount of rainfall received is approximately 125 mm. Therefore, $\Lambda_2(T,R)$ increases with an increase in rainfall up to 125 mm, but decreases with further increases in rainfall. Additionally, the temperature-dependent egg hatching rate $\alpha_J(T)$ represents the transition from the egg stage to the juvenile stage, while the juvenile maturation rate $\theta_J(T)$ signifies the transition from the juvenile stage to the adult stage. The regression lines that best fit the temperature data in SI Table S2 for these rates are represented by equation (19):

$$\left.\begin{aligned}\alpha_J(T) &= -0.0031084T^2 + 0.1775496T - 2.3562789\\ \theta_J(T) &= -0.0006839T^2 + 0.0385458T - 0.4990643\end{aligned}\right\} \tag{19}$$

Clearly, $1/\alpha_J(T)$ and $1/\theta_J(T)$ represents the lengths of time required for an egg to survive before hatching and for a juvenile snail to mature, respectively. As a result, the total time $t_S(T)$ needed for a snail cycle to develop from an egg to an adult snail can be calculated as $t_S(T) = [\alpha_J(T) + \theta_J(T)]/\alpha_J(T).\theta_J(T)$.

The snail recruitment rate $\Lambda_2(T,R)$ in equation (20) is derived by substituting equations (16)–(19) into equation (15).

$$\Lambda_2(T,R) = \frac{\left(-0.0031084T^2 + 0.1775496T - 2.3562789\right) \times \left(-0.0006839T^2 + 0.0385458T - 0.4990643\right)}{\left(-0.0031084T^2 + 0.1775496T - 2.3562789\right) + \left(-0.0006839T^2 + 0.0385458T - 0.4990643\right)}$$
$$\times \frac{-0.09601T^2 + 5.10696T - 59.52573}{1.120 \times 10^{-4}T^2 - 5.208 \times 10^{-3}T + 0.06332}$$
$$\times \left(4P_{ME} \Big/ R_L^2\right) R(R_L - R)$$
$$\times \left(4P_{MJ} \Big/ R_L^2\right) R(R_L - R)$$
$$\times e^{-\left(8.750 \times 10^{-5}T^2 - 3.762 \times 10^{-3}T - 0.043178\right)} \tag{20}$$

Consequently, equation (20) for $\Lambda_2(T,R)$ establishes a direct relationship between temperature, rainfall, and the transmission indicator R_0. The rate of change of R_0 with respect to temperature can be determined by $\frac{dR_0}{dT} = \frac{d\Lambda_2(T,R)}{dT}.\frac{dR_0}{d\Lambda_2(T,R)}$, while the rate of change of R_0 with respect to rainfall can be assessed using $\frac{dR_0}{dR} = \frac{d\Lambda_2(T,R)}{dR}.\frac{dR_0}{d\Lambda_2(T,R)}$. When $\frac{dR_0}{dT} < 0$, an increase in temperature leads to a decrease in R_0, particularly in areas affected by global warming. However, when $\frac{dR_0}{dT} > 0$, rising temperature results in both an increase in R_0 and the prevalence of the disease. Similarly, if $\frac{dR_0}{dR} < 0$, increased precipitation leads to a decrease in R_0, whereas if $\frac{dR_0}{dR} > 0$, higher precipitation leads to an increase in R_0 and disease prevalence.

The overall impact of temperature and/or rainfall on R_0 can be assessed by examining the combined effects of these factors. The following equations mathematically connect R_0 to temperature (T) and precipitation (R)

$$\frac{dR_0}{dT,R} = \frac{d\beta_1(T)}{dT}.\frac{dR_0}{d\beta_1(T)} + \frac{d\Lambda_2(T,R)}{dT}.\frac{dR_0}{d\Lambda_2(T,R)} + \frac{d\beta_2(T)}{dT}.\frac{dR_0}{d\beta_2(T)} + \frac{dd_v(T)}{dT}.\frac{dR_0}{dd_v(T)} + \frac{d\delta_2(T)}{dT}.\frac{dR_0}{d\delta_2(T)}$$

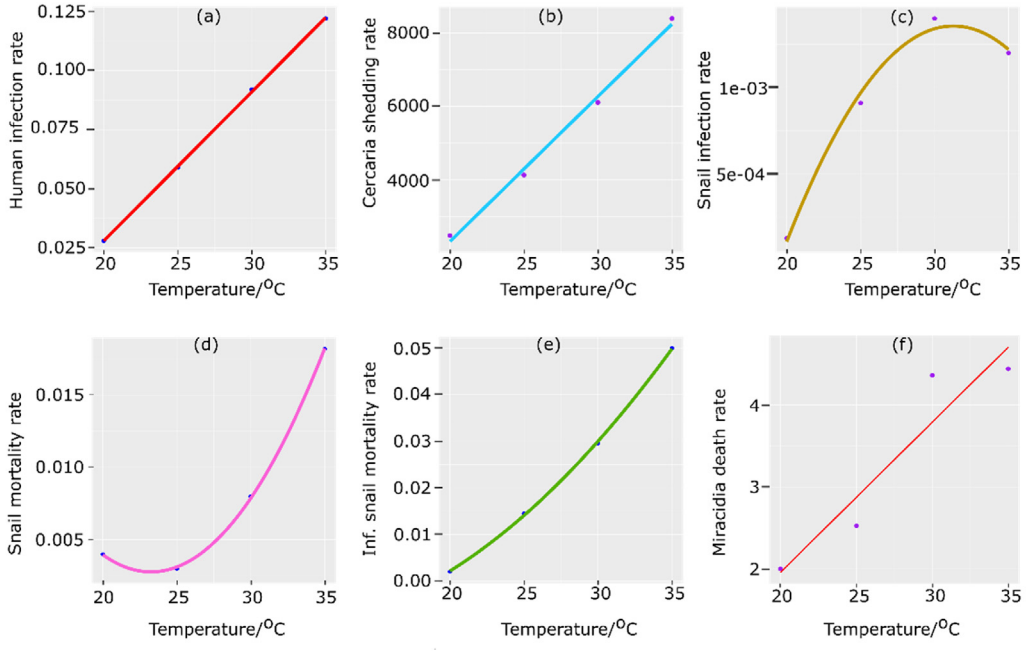

Fig. 2. Fitted models of temperature variant parameters; (a) human infection rate $\beta_1(T)$, (b) cercaria shedding rate $\omega_2(T)$, (c) snail infection rate $\beta_2(T)$, (d) snail mortality rate $d_v(T)$, (e) infected snail mortality rate $\delta_2(T)$, (f) miracidia death rate, $\upsilon_3(T)$ against temperature.

$$+\frac{d\upsilon_3(T)}{dT}.\frac{dR_0}{d\upsilon_3(T)}+\frac{d\omega_2(T)}{dT}.\frac{dR_0}{d\omega_2(T)}+\frac{d\Lambda_2(T,R)}{dR}.\frac{dR_0}{d\Lambda_2(T,R)}$$

Furthermore, when both temperature and precipitation increase simultaneously, the combined effects on R_0 are determined by the value of $\frac{d^2R_0}{dTdR}<0$. If $\frac{d^2R_0}{dTdR}>0$, R_0 increases as both temperature and precipitation rise. A higher value of R_0 indicates greater challenges in controlling the spread of schistosomiasis, while a lower value of R_0 makes it easier to combat the disease.

3.2. Numerical simulations

In this section, numerical simulations of the model system (1) are conducted to provide support, validation, and verification of the findings presented in the numerical analysis. Specifically, Fig. 2 illustrates the influence of temperature on specific parameters within the transmission dynamics of schistosomiasis.

Fig. 3 presents the impact of temperature and rainfall on specific parameters, which in turn affect the rate of snail recruitment and subsequent changes in disease transmission. Notably, the figure highlights that an increase in rainfall, up to a threshold of approximately 140 mm, is associated with an elevated probability of survival for both snail eggs and juveniles (Fig. 3e and f). This observation underscores the importance of rainfall in influencing the reproductive success and population dynamics of snails, thereby influencing the overall transmission of the disease.

The findings indicate that mean monthly temperatures of 22–27 °C (Table 2) are typical across the three countries. These temperatures are associated with high rates of schistosomiasis activity of different host snail traits and schistosomes (Fig. 4A–C; see also SI Figures S1, S3, S5), making them ideal conditions for the development of schistosomiasis and leading to high reproduction numbers (Fig. 4D). In addition, the human infection rate (Fig. 4A), snail infection rate (Fig. 4B), and snail recruitment rate (Fig. 4C) all peak around the same time of the year across the three countries. This typically happens during February and April and between the months of October and November, respectively, when the temperatures range between 23.7 and 26.7 °C. Infection levels in the area are at their lowest in July. The region also experiences monthly maximum temperatures ranging from 27 to 33 °C (Table 2), which severely restricts the activity of various host snail traits and schistosomes (see SI Figures S2, S4, and S6). As a result, there are generally fewer new cases of schistosomiasis overall in the region during this season (Fig. 4E).

The three nations have different annual rainfall patterns (Fig. 4F). Schistosomiasis cases increase in Uganda from March to May until the second rainy season, which lasts through the warm months of June and July and the rainy months of August to November. During this period, the endemic level of the disease remains almost unchanged until November, the beginning of the dry season, when numbers tend to decrease. During the dry months from April to July in Tanzania and April to September in Kenya, schistosomiasis cases decline. In Tanzania, cases begin to rise from August and peak in December and from January

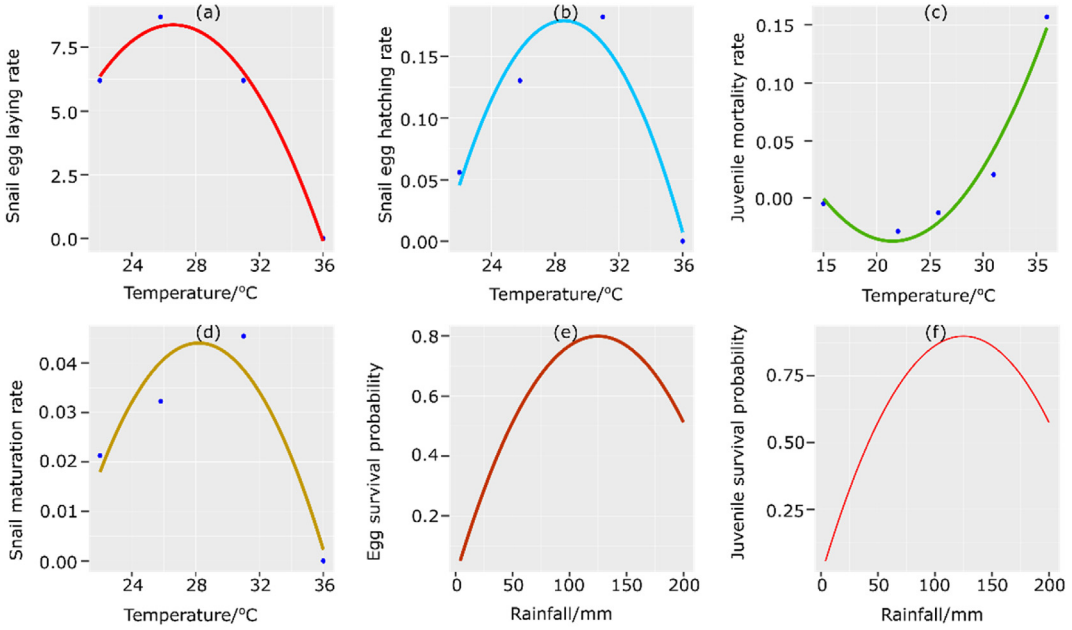

Fig. 3. Fitted model of temperature -and rainfall-dependent parameter simulations for (a) snail egg laying rate, $E_v(T)$, (b) snail egg hatching rate $\alpha_J(T)$, (c) juvenile mortality rate $\upsilon_j(T)$ (d) juvenile maturation rate $\theta_J(T)$, (f) egg survival probability $P_E(R)$, and (g) juvenile survival probability $P_j(R)$.

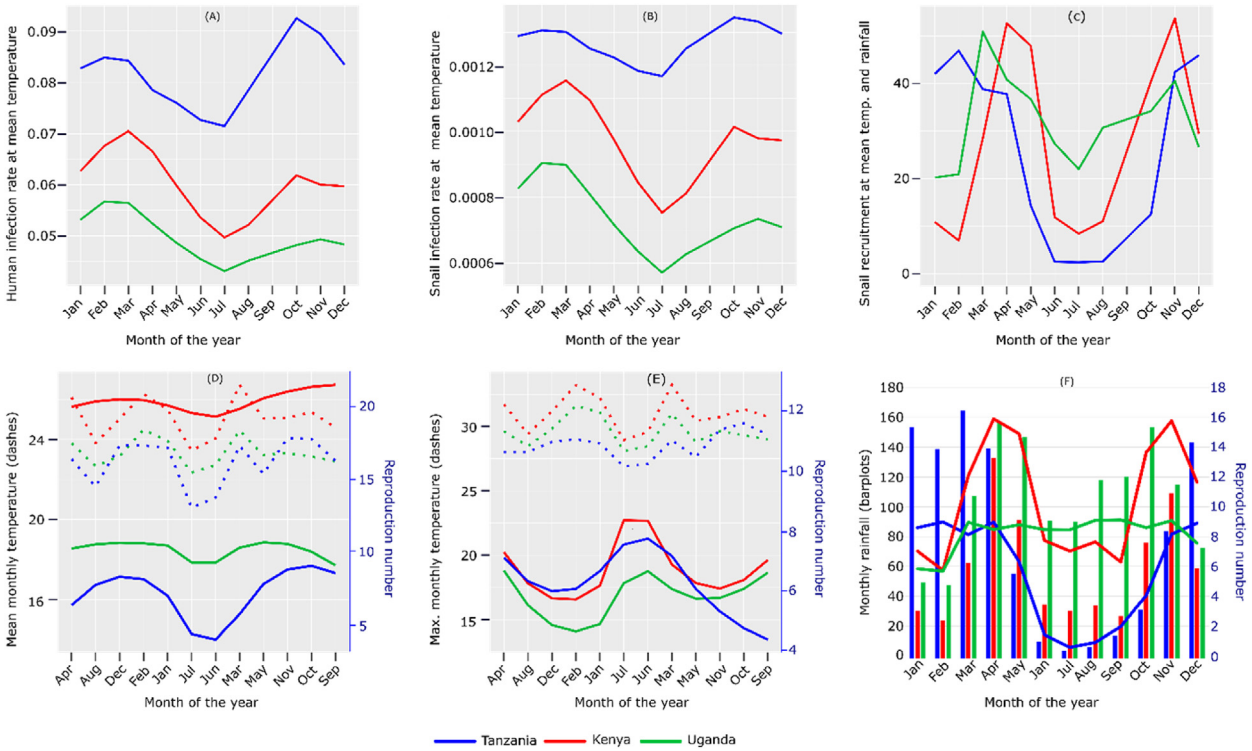

Fig. 4. Individual seasonal effects of temperature and/or rainfall on (A) human infection rate, (B) snail infection rate, (C) snail recruitment rate, and (D), (E), and (F) reproduction numbers in Tanzania (blue), Kenya (red), and Uganda (green). For other temperature- and/or precipitation-dependent parameters, see SI Figures S1–S6.

to April before they begin to decline. In Kenya, they rise from September to November and from February to April. In addition, the reproduction numbers in Kenya are so much higher (4D) and (4F) as compared to Tanzania and Uganda is associated with high rates of juvenile maturation (which enhance snail recruitment; Fig. 4C), cercaria shedding, snail egg laying and hatching rate (see SI Figures S1, S3, S5).

The schistosomiasis infection patterns are somewhat similar when temperature and rainfall are modelled together, with lowest values in July and August (Fig. 5A). However, patterns of peaks are different with two peaks for Tanzania and Kenya with rather similar phases in April (maximum) and a second maximum later in the year. A different annual pattern for Uganda with only one peak and a phase shift of the maximum towards an earlier seasonal peak through December, January till February. Surprising is the shear drop in Kenya from December to January. Fig. 5B depicts patterns that are quite similar to those in Fig. 5A for Kenya and Uganda, but behaviors in Tanzania changes after one season of infection, however, with similarly low case numbers through June, July and August as in Fig. 5A.

Schistosomiasis is a challenge across Tanzania, Kenya and Uganda, especially in March and April. For individual countries, the three months with the highest rates of infections are April, May, and December in Kenya; February, March, and December in Uganda; and April, and November in Tanzania (Fig. 5). During these months, the mean and maximum temperatures, and precipitation values in the three countries increase from 20.6 to 26.1 °C, 26.9–31.7 °C and from 5 to 165 mm, respectively. In contrast, there are relatively few cases in the three countries in June and July with mean, and maximum temperatures, and precipitation from 21.1 to 24.1 °C, 26.9–29.4 °C, and from 5.0 to 91.8 mm, respectively. For example, in Uganda, the infection numbers drop down to almost zero in Jul to Aug, while reproduction rates in Tanzania and Kenya are still around 6 to 7 during this time of the year (Fig. 5A). The maximum values in Kenya are around 50% higher in the peak season compared to Uganda and Tanzania (Fig. 5A). A comparison of precipitation with mean monthly temperatures (Fig. 5A) and maximum monthly temperatures (Fig. 5B) reveals that for Uganda, Tanzania, and Kenya, respectively, the peaks are approximately 9, 11, and 15 infections per day and 6, 7, 13 infections per day, respectively.

3.3. Expected future changes in temperature and precipitation

Tables 3 and 4 outline the temperature-and precipitation-related parameter variations across different future climate scenarios. Emphasis is placed on scenarios with severe temperatures that negatively impact schistosomiasis activity. Simulation results of crucial parameters for the persistence of schistosomiasis are presented in Table 5.

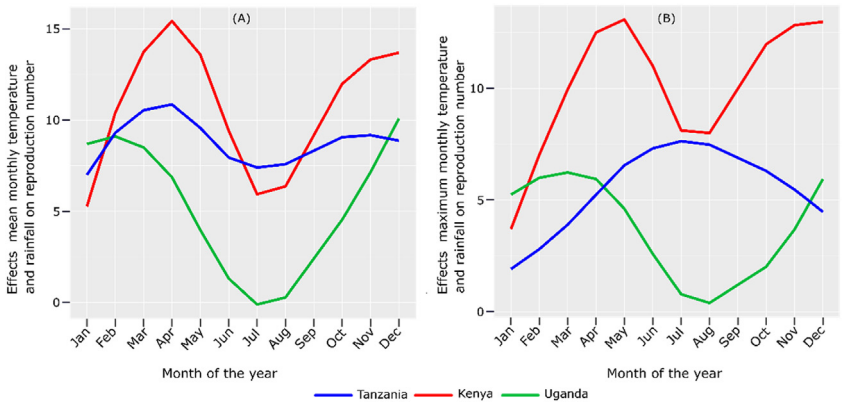

Fig. 5. Simultaneous effects of precipitation and mean temperature (A) as well as maximum temperatures (B) on reproduction numbers in Uganda (green), Kenya (red), and Tanzania (blue).

In the temperature range of [27, 35]°C, the findings indicate a decrease in parasite eggs, egg hatching rates, juvenile maturation rates, and snail recruitment rates with increasing temperatures (Table 3).

The findings demonstrate that temperatures ranging from 27 to 33 °C, combined with precipitation levels of 4–150 mm, create favorable conditions for snail recruitment. However, beyond 150 mm of rainfall, snail recruitment declines (Table 4).

The results of the PRCC test indicate that certain factors, such as the proportion of stools from infected individuals (ρ), the number of parasite eggs per gram per day (θ_h), the miracidia shedding rate per parasite egg (ω_1), and the snail recruitment rate $\Lambda_2(T,R)$, will continue to significantly influence disease transmission in the context of climate changes until 2050 (Table 5). An increase in these parameters leads to an elevated transmission of schistosomiasis. Among these factors, $\Lambda_2(T,R)$ is the only parameter that depends on both temperature and precipitation and is the most sensitive to changes. For instance, temperature ranges between 31 and 35 °C and rainfall levels between 100 and 200 mm, as well as seasons characterized by 4–50 mm of rainfall and temperatures of 27–29 °C, demonstrate that snail recruitment has a substantial impact on the reproduction number. The findings indicate that temperatures between 27 and 33 °C that occur along with precipitations of 4–150 mm are suitable for snail recruitment. Beyond 150 mm rainfall, snail recruitment declines (Table 4).

4. Discussion

Mechanistic models provide valuable insights into the incidence and burden of infectious diseases such as schistosomiasis. They enable tracking of short-term and long term effects on disease transmission and are particularly valuable for climate change assessment and projections. The mechanistic approach used in this study quantifies or understanding of relevant processes, enhancing confidence in extrapolating to various future conditions. Our model incorporates essential

Table 3
Model sensitivity of temperature- and precipitation-dependent parameter values. The full temperature range $[27,35]$°C is subdivided into intervals of 2 °C and the precipitation value is fixed at 100 mm when estimating the effect of temperature alone on snail recruitment rate $\Lambda_2(T,R)$, a temperature-and precipitation dependent parameter. Values are given a ranges and baseline values (*). Other parameter descriptions are given in SI Tables S1 and S2.

Temperature	β_1(T)	β_1^*	β_2(T)	β_2^*	d_v (T)	d_v^*	δ_2(T)	δ_2^*	ω_2(T)	ω_2^*	$\Lambda_2(T)_{100mm}$	$\Lambda_2^*(T)$
27-29 °C	0.0721	0.0784	0.001177	0.00124	0.0044	0.0055	0.0199	0.0232	5078	5473	43.7989	35.8646
	−0.0847		−0.001305		−0.0065		−0.0265		−5868		−27.9302	
29-31 °C	0.0847	0.091	0.001305	0.00133	0.0065	0.0080	0.0265	0.0301	5868	6263	27.9302	20.992
	−0.0973		−0.001355		−0.0095		−0.0336		−6658		−14.0545	
31-33 °C	0.0973	0.1036	0.001355	0.00134	0.0095	0.0115	0.0336	0.0375	6658	7053	14.0545	9.4959
	−0.1099		−0.001327		−0.0134		−0.0414		−7448		−4.9372	
33-35 °C	0.1099	0.1162	0.001327	0.00127	0.0134	0.0158	0.0414	0.0457	7448	7843	4.9372−0.5657	2.7515
	−0.1225		−00.001177		−0.0182		−0.0499		−8237			

Temperature	b_v (T)	b_v^*	$E_v(T)$	E_v^*	$\alpha_J(T)$	α_j^*	$\upsilon_j(T)$	υ_j^*	$\theta_J(T)$	θ_j^*	$u_3(T)$	u_3^*
27-29 °C	3.2418	3.4252	8.3709	8.1013	0.1715	0.1750	0.0039	0.0051	0.0432	0.0434	3.2418	3.4252
	−3.6086		−7.8317		−0.1785		−0.0062		−0.0436		−3.6086	
29-31 °C	3.6086	3.792	7.8317	7.1781	0.1785	0.1723	0.0062	0.0077	0.0436	0.0411	3.6086	3.7920
	−3.9754		−6.5244		−0.1606		−0.0092		−0.0386		−3.9754	
31-33 °C	3.9754	4.1588	6.5244	3.9867	0.1606	0.1392	0.0092	0.0110	0.0386	0.0334	3.9754	4.1588
	−4.3422		−4.4491		−0.1178		−0.0128		−0.0282		−4.3422	
33-35 °C	4.3422−4.709	4.5256	4.4491	3.02735	0.1178	0.1680	0.0128	0.0150	0.0282	0.0203	4.3422	4.5256
			−1.6056		−0.0502		−0.0172		−0.0123		−4.7090	

Table 4
Effects of precipitation at constant temperatures in the range of 27–35 °C on the snail recruitment rate. To account for variations between regions, precipitation of 4–200 mm is split into intervals of 50 mm.

T/°C	R/mm	$\Lambda_2(T,R)$	$\Lambda_2^*(T,R)$	T/°C	R/mm	$\Lambda_2(T,R)$	$\Lambda_2^*(T,R)$
	4–50	0.1885–12.4134	6.3009		4–50	0.0605–2.1943	1.1274
27-29 °C	50–100	19.4662–27.9302	23.6982	31-33 °C	50–100	6.2465–4.9372	5.5919
	100–150	43.7989–27.9302	21.8995		100–150	14.0545–4.9372	9.4959
	150–200	43.7989–12.4134	28.1062		150–200	14.0545–2.1943	8.1244
	4–50	0.1202–6.2465	3.1834		4–50	0.0212–0.2514	0.13630
29-31 °C	50–100	12.4134–14.0545	13.2339	33-35 °C	50–100	2.1943–0.5657	1.3800
	100–150	27.9302–14.0545	20.9924		100–150	4.9372–0.5657	2.751
	150–200	27.9302–6.2465	17.0884		150–200	4.9372–0.2514	2.5943

epidemiological and climate-dependent stages for intermediate hosts and *Schistosoma* parasites. Firstly, our model reveals that when the reproduction number is less than or equal to unity, a disease-free equilibrium is achieved, which is both locally and globally asymptotically stable. Conversely, when the reproduction number exceeds unity, a unique endemic equilibrium arises, which is locally asymptotically stable. Secondly, incorporating both temperature and precipitation into the model yields a better understanding of schistosomiasis transmission patterns compared to modeling them separately for the reproduction number of a given month. This demonstrates that the combined influence of temperature and precipitation provides a more comprehensive explanation of schistosomiasis transmission dynamics. The following discussions will present both the individual and combined effects of temperature and precipitation.

4.1. Effect of temperature

The study demonstrates that the transmission potential of schistosomiasis is highly sensitive to changes in the mean and maximum temperature within the region, leading to variations in the number of cases across seasons and months. This aligns with the well-established understanding that schistosomiasis, being a vector-borne disease, is greatly influenced by climatic fluctuations (Martens et al., 1995). Schistosomiasis infections exhibit changes in accordance with temperature variations within the mean monthly temperature range of 22–27 °C. Within this temperature range, there is an increase in human infection, snail infection rate, snail egg-laying rate, egg hatching, and snail maturation with rising temperatures. These findings are consistent with previous model-based studies by Ngarakana-Gwasira et al. (Ngarakana-Gwasira et al., 2016), which propose an optimal temperature range of 18–28 °C for schistosomiasis transmission. Additionally, Malone (Malone, 2005) reports a temperature range of 20–27 °C as ideal for the intramolluscan development of S. mansoni within Biomphalaria spp. snails. Moreover, Marti (Marti, 1986) and Manyangadze et al. (Manyangadze et al., 2016) observe an increase in the snail population with a slight temperature rise above 25 °C. Conversely, there are fewer cases of schistosomiasis in months with increasing mean monthly temperatures above 27 °C, corresponding to a decline in schistosomiasis activity. Similarly, monthly maximum temperatures between 27 and 33 °C are associated with reduced schistosomiasis cases, attributed to decreased survival of eggs and juveniles, lower rates of human and snail infection, and slower snail maturation. These findings align with the understanding that higher temperatures are linked to increased snail mortality, reduced fecundity, and hindered snail growth, resulting in a decline in schistosomiasis cases (McCreesh & Booth, 2013; Ngarakana-Gwasira et al., 2016; Kalinda et al., 2017b).

4.2. Effects of precipitation

The availability of suitable snail breeding sites, primarily in surface water such as ponds, is largely influenced by precipitation (Xue et al., 2011). Our findings suggest that moderate precipitation ranging from 5 to 150 mm may contribute to an increase in the number of schistosomiasis cases. This is associated with a higher snail recruitment rate, as snail eggs and juveniles have a greater chance of survival under such conditions. These results are consistent with previous studies that have shown a positive correlation between precipitation, the distribution of intermediate host snails, and the spread of schistosomiasis (Codjoe & Larbi, 2016; Stensgaard et al., 2016; Tabo et al., 2022; Xue et al., 2011). On the other hand, rainfall exceeding 150 mm has a suppressive effect on schistosomiasis transmission. This is attributed to a reduction in snail recruitment due to decreased survival of snail eggs and juveniles. This finding is supported by evidence demonstrating that decreased schistosomiasis cases result from increased streamflow velocities and associated habitat disturbance, which negatively impact the recruitment and survival of cercariae, miracidia, snail eggs, and juveniles (Adekiya et al., 2020; Xue et al., 2011). Furthermore, during the rainy season, there is a potential decrease in activities related to infested water, such as swimming, fishing, sports, and water collection for household use, due to flood-related risks. This could also contribute to a reduction in schistosomiasis transmission.

Table 5
PRCC values for the temperature and precipitation dependent parameters, with temperature values 27 – 35°C and precipitation in the range of [4, 200] mm and R_0 as a response function. The three most crucial factors affecting the dynamics of the model at such adverse temperatures are indicated in bold.

parameter	27-29 °C				29-31 °C				31-33 °C				33-35 °C			
	4 −50 mm	50 −100 mm	100 −150 mm	150 −200 mm	4 −50 mm	50 −100 mm	100 −150 mm		4 −50 mm	50 −100 mm	100 −150 mm	100 −200 mm	4 −50 mm	50 −100 mm	100 −150 mm	100 −200 mm
Λ_1	0.19062	0.18278	0.19587	0.16006	0.19081	0.19007	0.19826		0.19248	0.1939	0.20199	0.1988	0.1978	0.2033	0.1992	0.1963
τ	0.0321	0.02908	0.0297	0.03287	−0.0036	0.02412	0.01696		−0.6059	−0.6669	0.01209	0.0038	−0.001	0.00731	0.0005	0.5010
δ_1	−0.5544	−0.6483	−0.6455	−0.6139	−0.6010	−0.6602	−0.6578		−0.0035	0.0227	−0.6551	−0.632	−0.618	−0.646	0.6244	−0.6111
υ_1	−0.1351	−0.1493	−0.1491	−0.1437	−0.1469	−0.1501	−0.1518		−0.1469	−0.1528	−0.1532	−0.151	−0.148	−0.1511	−0.1485	−0.1469
ρ	**0.4875**	**0.5505**	**0.54872**	**0.52656**	**0.49145**	**0.5564**	**0.55024**		**0.4944**	**0.5599**	**0.5443**	**0.5208**	**0.5080**	**0.5359**	**0.51419**	−0.0029
θ_h	**0.75669**	**0.82174**	**0.8205**	**0.8007**	**0.7544**	**0.82665**	**0.81948**		**0.7586**	**0.8293**	**0.8133**	**0.7887**	**0.7736**	**0.8036**	**0.7805**	**0.7651**
ω_1	**0.9452**	**0.9632**	**0.9628**	**0.9577**	**0.9478**	**0.96467**	**0.9634**		**0.9491**	**0.9654**	**0.9622**	**0.9567**	**0.9528**	**0.9600**	**0.9545**	**0.9507**
υ_2	0.03214	0.0291	0.02970	0.03287	−0.0036	0.02412	0.0169		−0.0035	0.0227	0.01209	0.0038	−0.001	0.0073	0.0005	−0.0029
υ_4	0.03214	0.02908	0.02970	0.03287	−0.0036	0.02412	0.01696		−0.0034	0.0227	0.01209	0.0038	−0.001	0.0073	0.0005	−0.0029
N_E	0.03214	0.02908	0.02970	0.03287	−0.0036	0.02412	0.01696		−0.0034	0.0227	0.01209	0.0038	−0.001	0.0073	0.0005	−0.0029
$\beta_1(T)$	0.0871	0.11411	0.10389	0.09323	0.01239	0.1178	0.0926		−0.0143	0.0793	0.04083	0.0109	−0.009	0.0195	−0.0047	−0.0169
$\beta_2(T)$	0.08422	0.12706	0.12478	0.10512	0.16364	0.14316	0.15494		0.1113	0.0792	0.09726	0.1057	0.1753	0.1744	0.1754	0.1751
$d_v(T)$	−0.3147	−0.4065	−0.40306	−0.3686	−0.3772	−0.4256	−0.4275		0.3583	−0.4053	−0.4001	−0.381	−0.344	−0.3657	−0.3484	0.3373
$\delta_2(T)$	−0.1228	−0.1735	−0.17043	−0.14752	−0.2066	−0.1932	−0.2051		−0.1621	−0.1408	−0.1564	−0.161	0.147	−0.1431	−0.1466	−0.1479
$\omega_2(T)$	0.00799	0.06156	0.05783	0.03218	0.1578	0.07899	0.1065		0.1373	0.0587	0.09742	0.1212	0.1217	0.0992	0.1179	0.1265
$\upsilon_3(T)$	−0.0813	−0.0812	−0.0813	−0.0797	−0.0729	−0.0773	−0.0786		−0.0621	−0.0637	−0.0654	−0.064	−0.058	−0.0599	0.059	−0.0572
$\Lambda_2(T,R)$	**0.78953**	**0.2717**	**0.30385**	**0.63269**	**0.76732**	**0.07739**	**0.4321**		**0.7657**	**0.1584**	**0.5681**	**0.7031**	**0.7400**	**0.6382**	**0.7251**	**0.7554**

4.3. Effects of temperature and precipitation

Our study highlights the importance of suitable monthly temperature and precipitation conditions in maximizing the transmission of schistosomiasis. These findings support previous research indicating that temperature and precipitation play crucial roles in species richness (Hauffe et al., 2016), the distribution of intermediate host snails (Tabo et al., 2022), and the size of snail populations, ultimately influencing disease transmission patterns and spread (McCreesh & Booth, 2013; Stensgaard et al., 2016). We demonstrate that regions in Uganda, Tanzania, and Kenya are most susceptible to schistosomiasis transmission and spread when they experience temperature variations within the range of 20–27 °C and varying levels of rainfall between 5 and 140 mm. This aligns with observations made by Martens et al. (Martens et al., 1995), McCreesh and Booth (McCreesh & Booth, 2013), and Stensgaard et al. (Stensgaard et al., 2016), highlighting the favorable conditions for schistosomiasis transmission resulting from climate change when these specific hydrometeorological conditions are met. Interestingly, our results indicate that regions with adverse temperatures exceeding 27 °C, which are typically known to limit schistosomiasis transmission, may still facilitate disease development when accompanied by suitable precipitation. In such regions characterized by a combination of dry and wet weather conditions, episodes of precipitation followed by a drop in temperatures below 27 °C create favorable environmental conditions for schistosomiasis transmission. However, it is worth noting that certain ranges of precipitation variation may have no discernible effect on temperature and may even limit the development of schistosomiasis, resulting in a decline in reported cases. This observation provides corroboration for the findings in the scientific literature, which propose that certain weather patterns may not favor schistosomiasis transmission due to their limited influence on average temperatures in specific regions (Mas-Coma et al., 2009; McCreesh & Booth, 2013; Van der Wiel & Bintanja, 2021; Tabo et al., 2023). When considered collectively, the transmission dynamics of schistosomiasis are susceptible to seasonal variations influenced by climate factors, potentially exerting significant effects on the efficacy of control and elimination endeavors.

4.4. Future trend of schistosomiasis

The impact of climate change on schistosomiasis transmission and control measures varies depending on the frequency, temporal distribution, and range of temperature and rainfall events. Climate change-induced increases in snail recruitment rates are expected to lead to higher schistosomiasis cases during specific seasons. This finding aligns with analogous models that predict the expansion of

schistosomiasis into cooler regions and the potential for increased transmission in the future (Martens et al., 1995; McCreesh et al., 2015). Our model results suggest that seasons characterized by high snail recruitment rates present optimal opportunities to intensify intermediate host snail control efforts. However, in regions experiencing precipitation levels ranging from 50 to 150 mm and average temperature fluctuations between 27 and 35 °C, the PRCC test results indicate that snail recruitment rate values remain constrained and may not significantly drive schistosomiasis occurrence. This suggests that the impact of precipitation fluctuations within this range on the temperature-constrained snail recruitment is minimal, consistent with observations that rainfall between 50 and 150 mm is negatively correlated with a low number of *S. mansoni* patients (Xue et al., 2011). In summary, our parameterized models of schistosomiasis and climate dynamics provide insights into regions that may become more conducive to the spread of the disease in the future. This information is valuable for identifying areas that may require heightened surveillance and targeted control interventions to mitigate the potential impact of climate change on schistosomiasis transmission.

4.5. Model limitations/methodological implication and future research

It is important to acknowledge the limitations of our study. Firstly, the parameter values utilized in our model, which represent the biological aspects and real-life scenarios of schistosomiasis transmission, were sourced from the published literature. Consequently, inconsistencies and variability may exist within the data collected under diverse conditions, introducing potential uncertainties and biases into our model results. Nonetheless, the mathematical model employed in our manuscript offers a robust framework for comprehending the interplay between temperature, rainfall, and schistosomiasis transmission dynamics. It serves as a quantitative framework, with baseline parameter values providing a reasonable approximation, thereby enhancing our understanding of the impact of climate factors, seasons, and timing of interventions. By accurately predicting disease outbreaks, we facilitate the assessment of appropriate intervention strategies during specific months and seasons. Furthermore, this model has global applicability, extending its usefulness to diverse regions worldwide. In addition, our transmission model has been autonomous under static conditions. Despite insights gained, it is not exhaustive, and environmental variability and uncertainty persist. These result from natural fluctuations, parameter estimation, or external data sources. Fully addressing uncertainty and variability exceeds the scope of this paper. Future research should extend to a non-autonomous model, treating temperature and rainfall as dynamic variables. This extended model may introduce compartments for exposed, latent, and immature/juvenile snail populations and explore additional control measures other than climate.

5. Conclusion

Understanding the impact of climate change on schistosomiasis transmission requires considering the individual and combined effects of temperature and precipitation. When examined separately, the findings indicated that increasing mean monthly temperatures are associated with higher schistosomiasis cases, while increasing maximum monthly temperatures are linked to a decrease in cases. Additionally, a threshold level of rainfall is necessary to reduce the burden of schistosomiasis. However, the highest disease burden occurs when favorable temperature and precipitation conditions coincide, leading to increased prevalence of intermediate hosts, higher human and snail infection rates, enhanced survival of snail eggs and juveniles, and increased snail egg laying and hatching rates. These conditions also provide optimal opportunities for implementing control measures. Our model effectively identifies hydrometeorological conditions that increase the transmission risk of schistosomiasis, making it a valuable tool for predicting the spatial distribution of the disease under climate change and developing management strategies. This study contributes to the understanding of schistosomiasis transmission dynamics in the context of climate change and provides insights for policymakers to make informed decisions regarding disease control. Future research should explore the contrast between climate-driven management of snail vectors and schistosomiasis control strategies. Moreover, incorporating spatially explicit transmission models will enhance predictions of disease persistence and spread.

Ethics approval and consent to participate

Not applicable.

Consent for publication

Not applicable.

Funding

DAAD provided ZT with a PhD scholarship (Grant No. 57507871). As part of CK's postdoctoral training, he was awarded a scholarship from the Alexander von Humboldt Foundation (Grant No. ZMB1217528GF-P). There was no involvement of the funders in the design of the study, the collection or analysis of data, the decision to publish, or the preparation of the manuscript.

Availability of data and material

All data generated or analysed during this study are included in this published article and its supplementary information file (SI).

CRediT authorship contribution statement

Zadoki Tabo: Conceptualization, Data curation, Formal analysis, Investigation, Methodology, Software, Validation, Visualization, Writing – original draft. **Chester Kalinda:** Data curation, Methodology, Writing – review & editing. **Lutz Breuer:** Project administration, Resources, Supervision, Writing – review & editing. **Christian Albrecht:** Project administration, Resources, Supervision, Writing – review & editing.

Declaration of competing interest

The authors declare that they have no known competing financial interests or personal relationships that could have appeared to influence the work reported in this paper.

Acknowledgements

The authors extend their appreciation to the German Academic Exchange Service (DAAD) for awarding ZT a PhD scholarship (grant No. 57507871), as well as to the Alexander von Humboldt Foundation for generously supporting CK with a postdoctoral scholarship (grant No. ZMB1217528GF-P). Additionally, the authors would like to acknowledge Livingstone S. Luboobi from Makerere University for his invaluable guidance and expert advice on mathematical formulations.

Appendix A. Supplementary data

Supplementary data to this article can be found online at https://doi.org/10.1016/j.idm.2023.12.003.

References

Adekiya, T. A., Aruleba, R. T., Oyinloye, B. E., Okosun, K. O., & Kappo, A. P. (2020). The effect of climate change and the snail-schistosome cycle in transmission and bio-control of schistosomiasis in Sub-Saharan Africa. *International Journal of Environmental Research and Public Health, 17*(1), 181. https://doi.org/10.3390/ijerph17010181

Bergquist, R., Zhou, X. N., Rollinson, D., Reinhard-Rupp, J., & Klohe, K. (2017). Elimination of schistosomiasis: The tools required. *Infectious Diseases of Poverty, 6*, 1–9. https://doi.org/10.1186/s40249-017-0370-7

Castillo-Chavez, C., & Song, B. (2004). Dynamical models of tuberculosis and their applications. *Mathematical Biosciences and Engineering, 1*(2), 361–404. https://doi.org/10.3934/mbe.2004.1.361

Chavez, C. C., Feng, Z., & Huang, W. (2002). On the computation of R0 and its role on global stability. *Mathematical Approaches for Emerging and Re-emerging Infection Diseases: An Introduction, 125*, 31–65.

Chen, Z., Zou, L., Shen, D., Zhang, W., & Ruan, S. (2010). Mathematical modelling and control of schistosomiasis in hubei province, China. *Acta Tropica, 115*(1–2), 119–125. https://doi.org/10.1016/j.actatropica.2010.02.012

Codjoe, S. N. A., & Larbi, R. T. (2016). Climate change/variability and schistosomiasis transmission in Ga district, Ghana. *Climate & Development, 8*(1), 58–71. https://doi.org/10.1080/17565529.2014.998603

Colley, D. G., Bustinduy, A. L., Secor, W. E., & King, C. H. (2014). Human schistosomiasis. *The Lancet, 383*(9936), 2253–2264. https://doi.org/10.1016/S0140-6736(13)61949-2

Diekmann, O., Heesterbeek, J. A. P., & Metz, J. A. (1990). On the definition and the computation of the basic reproduction ratio R 0 in models for infectious diseases in heterogeneous populations. *Journal of Mathematical Biology, 28*, 365–382. https://doi.org/10.1007/BF00178324

Driessche, P., & Watmough, J. (2002). Reproduction numbers and sub-threshold endemic equilibria for compartmental models of disease transmission. *Mathematical Biosciences, 180*(1–2), 29–48. https://doi.org/10.1016/S0025-5564(02)00108-6

Feng, Z., Eppert, A., Milner, F. A., & Minchella, D. J. (2004). Estimation of parameters governing the transmission dynamics of schistosomes. *Applied Mathematics Letters, 17*(10), 1105–1112. https://www.sciencedirect.com/science/article/pii/S0893965904816884.

Fulford, A. J. C., Butterworth, A. E., Ouma, J. H., & Sturrock, R. F. (1995). A statistical approach to schistosome population dynamics and estimation of the life-span of Schistosoma mansoni in man. *Parasitology, 110*(3), 307–316. https://doi.org/10.1017/S0031182000080896

Gryseels, B., Polman, K., Clerinx, J., & Kestens, L. (2006). Human schistosomiasis. *The Lancet, 368*(9541), 1106–1118. https://doi.org/10.1016/S0140-6736(06)69440-3

Hauffe, T., Schultheiß, R., Van Bocxlaer, B., Prömmel, K., & Albrecht, C. (2016). Environmental heterogeneity predicts species richness of freshwater mollusks in sub-Saharan Africa. *International Journal of Earth Sciences, 105*, 1795–1810. https://doi.org/10.1007/s00531-014-1109-3

Home. (2023). *Climate change knowledge portal, World Bank climate change*. WBC. Available at: https://Climateknowledgeportal.Worldbank.Org/Country, 14 Febuary 2023.

Kalinda, C., Chimbari, M. J., Grant, W. E., Wang, H. H., Odhiambo, J. N., & Mukaratirwa, S. (2018). Simulation of population dynamics of Bulinus globosus: Effects of environmental temperature on production of Schistosoma haematobium cercariae. *PLoS Neglected Tropical Diseases, 12*(8), Article e0006651. https://doi.org/10.1371/journal.pntd.0006651

Kalinda, C., Chimbari, M. J., & Mukaratirwa, S. (2017a). Effect of temperature on the Bulinus globosus-Schistosoma haematobium system. *Infectious Diseases of Poverty, 6*(1), 1–7. https://doi.org/10.1186/S40249-017-0260-Z

Kalinda, C., Chimbari, M., & Mukaratirwa, S. (2017b). Implications of changing temperatures on the growth, fecundity and survival of intermediate host snails of schistosomiasis: A systematic review. *International Journal of Environmental Research and Public Health, 14*(1), 80. https://doi.org/10.3390/ijerph14010080

Kalinda, C., Mushayabasa, S., Chimbari, M. J., & Mukaratirwa, S. (2019). Optimal control applied to a temperature dependent schistosomiasis model. *Biosystems, 175*, 47–56. https://doi.org/10.1016/J.biosystems.2018.11.008

Liang, S., Spear, R. C., Seto, E., Hubbard, A., & Qiu, D. (2005). A multi-group model of Schistosoma japonicum transmission dynamics and control: Model calibration and control prediction. *Tropical Medicine and International Health, 10*(3), 263–278. https://doi.org/10.1111/j.1365-3156.2005.01386.x

Li, Y., Teng, Z., Ruan, S., Li, M., & Feng, X. (2017). A mathematical model for the seasonal transmission of schistosomiasis in the lake and marshland regions of China. *Mathematical Biosciences and Engineering, 14*(5–6), 1279–1299. https://doi.org/10.3934/mbe.2017066

Malone, J. B. (2005). Biology-based mapping of vector-borne parasites by geographic information systems and remote sensing. *Parassitologia, 47*(1), 27.

Mangal, T. D., Paterson, S., & Fenton, A. (2008). Predicting the impact of long-term temperature changes on the epidemiology and control of schistosomiasis: A mechanistic model. *PLoS One, 3*(1), e1438. https://doi.org/10.1371/journal.pone.0001438

Manyangadze, T., Chimbari, M. J., Gebreslasie, M., Ceccato, P., & Mukaratirwa, S. (2016). Modelling the spatial and seasonal distribution of suitable habitats of schistosomiasis intermediate host snails using Maxent in Ndumo area, KwaZulu-Natal Province, South Africa. *Parasites & Vectors, 9*(1), 1–10. https://doi.org/10.1186/s13071-016-1834-5

Martens, W. J. M., Jetten, T. H., Rotmans, J., & Niessen, L. W. (1995). Climate change and vector-borne diseases: A global modelling perspective. *Global Environmental Change, 5*(3), 195–209. https://doi.org/10.1016/0959-3780(95)00051-O

Marti, H. (1986). Field observations on the population dynamics of Bulinus globosus, the intermediate host of Schistosoma haematobium in the Ifakara area, Tanzania. *The Journal of Parasitology*, 119–124. https://doi.org/10.2307/3281803

Mas-Coma, S., Valero, M. A., & Bargues, M. D. (2009). Climate change effects on trematodiases, with emphasis on zoonotic fascioliasis and schistosomiasis. *Veterinary Parasitology, 163*(4), 264–280. https://doi.org/10.1016/j.vetpar.2009.03.024

McCreesh, N., & Booth, M. (2013). Challenges in predicting the effects of climate change on Schistosoma mansoni and Schistosoma haematobium transmission potential. *Trends in Parasitology, 29*(11), 548–555. https://doi.org/10.1016/j.pt.2013.08.007

McCreesh, N., Nikulin, G., & Booth, M. (2015). Predicting the effects of climate change on Schistosoma mansoni transmission in eastern Africa. *Parasites & Vectors, 8*, 1–9. https://doi.org/10.1186/S13071-014-0617-0

Michaels, R. M., & Prata, A. (1968). Evolution and characteristics of Schistosoma mansoni eggs laid in vitro. *The Journal of Parasitology*, 921–930. https://www.jstor.org/stable/3277120.

Najjuma, M., Nimusiima, A., Sabiiti, G., & Opio, R. (2021). Characterization of historical and future drought in central Uganda using CHIRPS rainfall and RACMO22T model data. *International Journal of Agriculture and Forestry, 11*, 9–15. https://doi.org/10.5923/j.ijaf.20211101.02

Ngarakana-Gwasira, E. T., Bhunu, C. P., Masocha, M., & Mashonjowa, E. (2016). Transmission dynamics of schistosomiasis in Zimbabwe: A mathematical and GIS approach. *Communications in Nonlinear Science and Numerical Simulation, 35*, 137–147. https://doi.org/10.1016/j.cnsns.2015.11.005

Ngoma, H., Wen, W., Ojara, M., & Ayugi, B. (2021). Assessing current and future spatiotemporal precipitation variability and trends over Uganda, East Africa, based on CHIRPS and regional climate model datasets. *Meteorology and Atmospheric Physics, 133*, 823–843. https://doi.org/10.1007/S00703-021-00784-3

Okuneye, K., & Gumel, A. B. (2017). Analysis of a temperature-and rainfall-dependent model for malaria transmission dynamics. *Mathematical Biosciences, 287*, 72–92. https://doi.org/10.1016/j.mbs.2016.03.013

Parham, P. E., & Michael, E. (2010). Modeling the effects of weather and climate change on malaria transmission. *Environmental Health Perspectives, 118*(5), 620–626. https://doi.org/10.1289/EHP.0901256

Schrader, M., Hauffe, T., Zhang, Z., Davis, G. M., Jopp, F., Remais, J. V., & Wilke, T. (2013). Spatially explicit modeling of schistosomiasis risk in eastern China based on a synthesis of epidemiological, environmental and intermediate host genetic data. *PLoS Neglected Tropical Diseases, 7*(7), Article e2327. https://doi.org/10.1371/journal.pntd.0002327

Soetaert, K., Petzoldt, T., & Setzer, R. W. (2010). Package deSolve: Solving initial value differential equations in R. *Journal of Statistical Software, 33*(9), 1–25. http://th.archive.ubuntu.com/cran/web/packages/deSolve/vignettes/deSolve.pdf.

Solomon, S. (Ed.). (2007), *Working group I contribution to the fourth assessment report of the IPCC: 4. Climate change 2007-the physical science basis*. Cambridge university press.

Steinmann, P., Keiser, J., Bos, R., Tanner, M., & Utzinger, J. (2006). Schistosomiasis and water resources development: Systematic review, meta-analysis, and estimates of people at risk. *The Lancet Infectious Diseases, 6*(7), 411–425. https://doi.org/10.1016/S1473-3099(06)70521-7

Stensgaard, A. S., Booth, M., Nikulin, G., & McCreesh, N. (2016). Combining process-based and correlative models improves predictions of climate change effects on Schistosoma mansoni transmission in eastern Africa. *Geospatial health, 11*, 94–101. https://doi.org/10.4081/gh.2016.406

Tabo, Z., Kalinda, C., Breuer, L., & Albrecht, C. (2023). Adapting strategies for effective schistosomiasis prevention: A mathematical modeling approach. *Mathematics, 11*(12), 2609. https://doi.org/10.3390/math11122609

Tabo, Z., Neubauer, T. A., Tumwebaze, I., Stelbrink, B., Breuer, L., Hammoud, C., & Albrect, A. (2022). Factors controlling the distribution of intermediate host snails of schistosoma in crater lakes in Uganda: A machine learning approach. *Frontiers in Environmental Science, 10*, Article 871735. https://doi.org/10.3389/fenvs.2022.871735

Team, R. C. (2018). *A language and environment for statistical computing*. Vienna, Austria: R Foundation for Statistical Computing. *Available online:* www.R-project.org/. (Accessed 11 September 2020).

Utzinger, J., Raso, G., Brooker, S., De Savigny, D., Tanner, M., Ørnbjerg, N., Singer, B. H., & N'goran, E. (2009). Schistosomiasis and neglected tropical diseases: Towards integrated and sustainable control and a word of caution. *Parasitology, 136*(13), 1859–1874. https://doi.org/10.1017/S0031182009991600

Van der Wiel, K., & Bintanja, R. (2021). Contribution of climatic changes in mean and variability to monthly temperature and precipitation extremes. *Communications Earth & Environment, 2*(1), 1. https://doi.org/10.1038/s43247-020-00077-4

Xue, Z., Gebremichael, M., Ahmad, R., Weldu, M. L., & Bagtzoglou, A. C. (2011). *Impact of temperature and precipitation on propagation of intestinal schistosomiasis in an irrigated region in Ethiopia: Suitability of satellite datasets*. https://doi.org/10.1111/j.1365-3156.2011.02820.x